Supplementary Information

Synthesis of $[Mn^{III}_{12}Mn^{II}_{6}(O)_6(OH)_2(OMe)_6(L)_4(LH)_2Br_{12}]$ (1)

$MnBr_2{\cdot}4H_2O$ (143.4 mg, 0.5 mmol) was added to 10 mL of a 0.05 M solution of LH_3 in MeOH. Upon the addition, the solution turns brown. The solution was stirred for 30 minutes after which it was filtered and allowed to stand. Dark black crystals suitable for *X*-ray analysis grew after two days. Elemental Analysis (%) calculated for **1**, $C_{70}H_{170}Mn_{18}N_{18}O_{42}Br_{12}$ (M = 3884.07): Mn, 25.46%; C, 21.65%; H, 4.41%; N, 3.26%. Found: Mn, 24.97%; C, 21.37%; H, 4.28%; N, 3.05%. Yield: 10-20%.

Crystallographic data

Crystal data for **1** (CCDC 2054790): $C_{70}H_{170}Mn_{18}N_{18}O_{42}Br_{12}$, M = 3884.07, 0.05 × 0.05 × 0.02 mm^3, monoclinic, space group $I2/a$ (No. 15), a = 18.408(6) Å, b = 23.209(7) Å, c = 30.524(12) Å, β = 90.126(5)°, $\alpha = \gamma = 90°$, V = 13041(7) $Å^3$, T = 100.0 K, Z = 4. Diamond Light Source I-19 EH1 diffractometer,[1] synchrotron radiation, λ = 0.68890 Å, T = 100.00 K, 2ϑmax = 40.249°, 46537 reflections measured, 6837 unique (R_{int} = 0.0984) which were used in all calculations. Final GooF = 1.071, wR_2 was 0.3459 (all data) and R_1 was 0.1163 (I≥2 σ(I)).

Magnetometry

Dc magnetic susceptibility and magnetisation measurements were performed on a freshly prepare microcrystalline, powdered sample of **1** on a Quantum Design SQUID MPMS-XL magnetometer equipped with a 7T magnet. Unit cell parameters were checked prior to sample preparation.

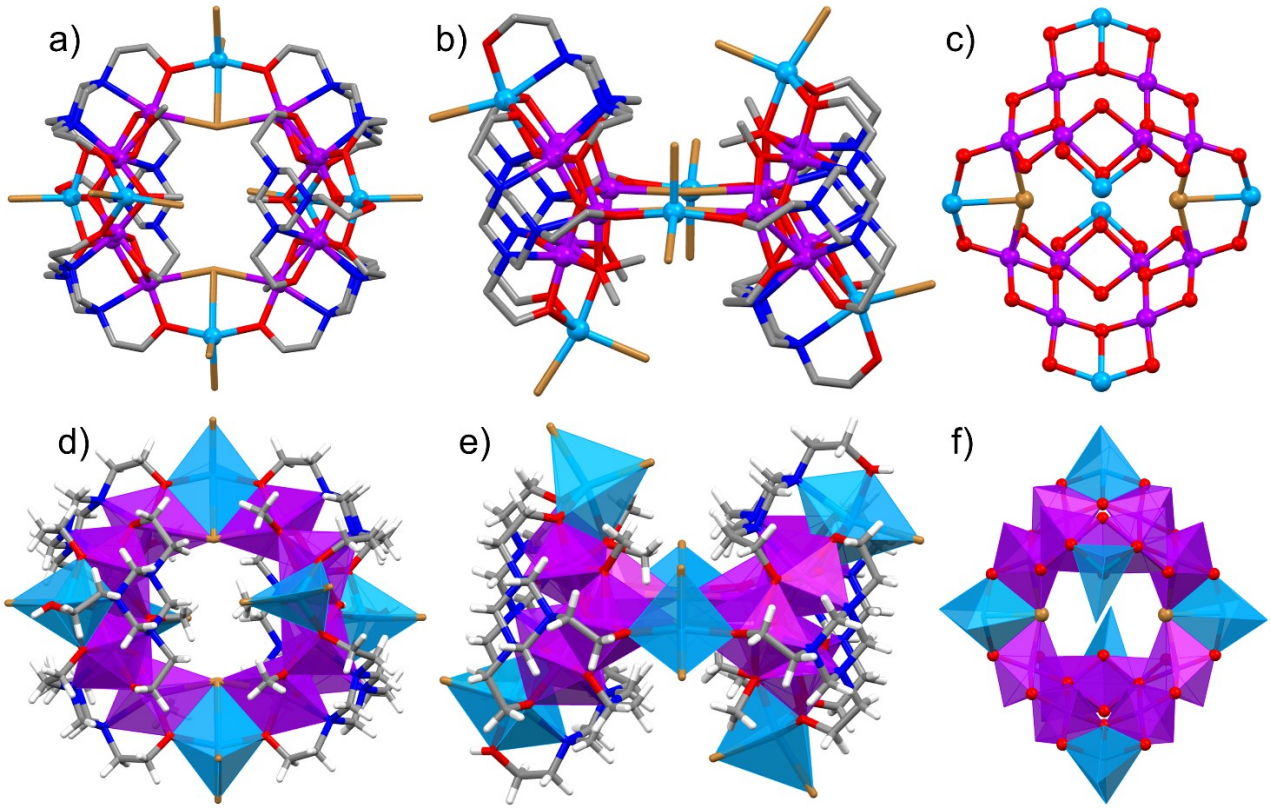

Figure S1. a)-b) Orthogonal views of the structure of **1**. c) Core of 1 highlighting the role of the bridging O- and Br- atoms. d)-e) Orthogonal polyhedral representations of the structure of 1 highlighting the role of the triazatriol ligand. Core of 1 in polyhedral format. Colour code: Mn^{III} = purple, Mn^{II} = light blue, O = red, Br = brown. H atoms omitted, except in d)-e).

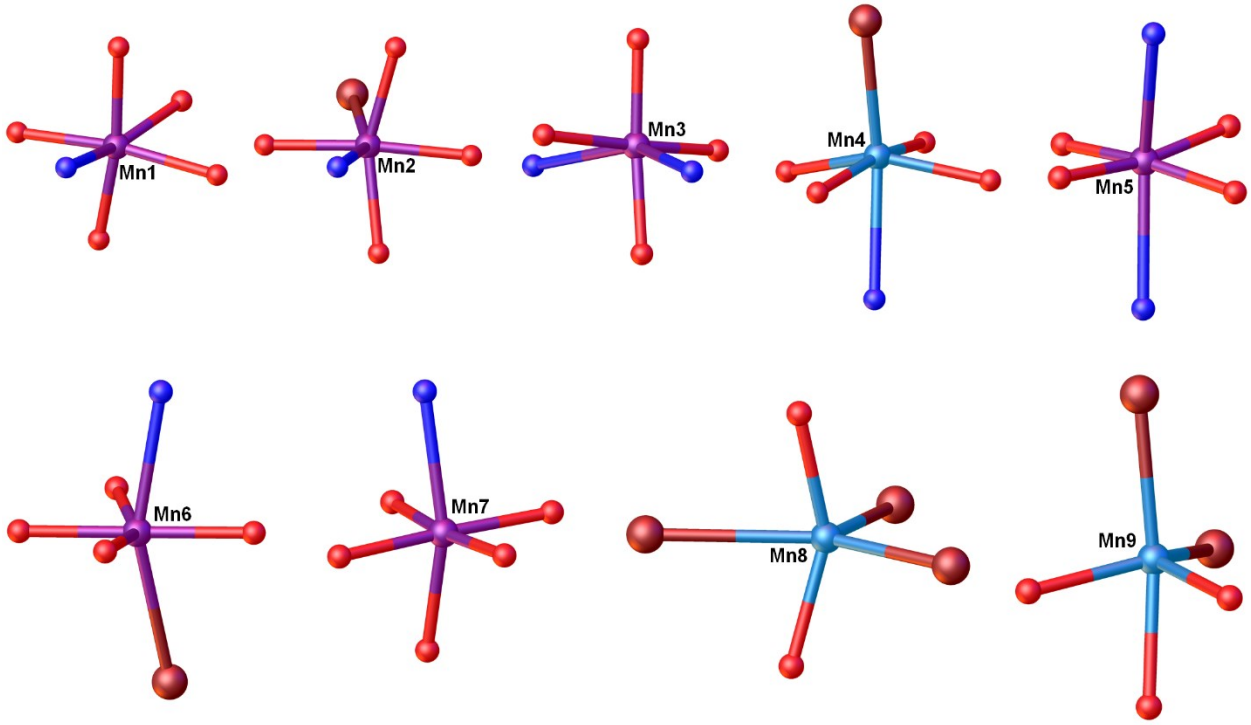

Figure S2. Coordination geometries of the nine independent Mn ions (Mn1-9) in the asymmetric unit of **1**. Mn1 = six coordinate octahedral {MnO_5N}; Mn2 = six coordinate, octahedral {MnO_5N}; Mn3 = six coordinate, octahedral {MnO_4N_2}; Mn4 = five coordinate, trigonal bipyramidal {MnO_3NBr}; Mn5 = six coordinate, octahedral {MnO_4N_2}; Mn6 = six coordinate, octahedral {MnO_4NBr}; Mn7 = six coordinate, octahedral {MnO_5N}; Mn8 = five coordinate, trigonal bipyramidal {MnO_2Br_3}; Mn9 = five coordinate, trigonal bipyramidal {MnO_2Br_3}.

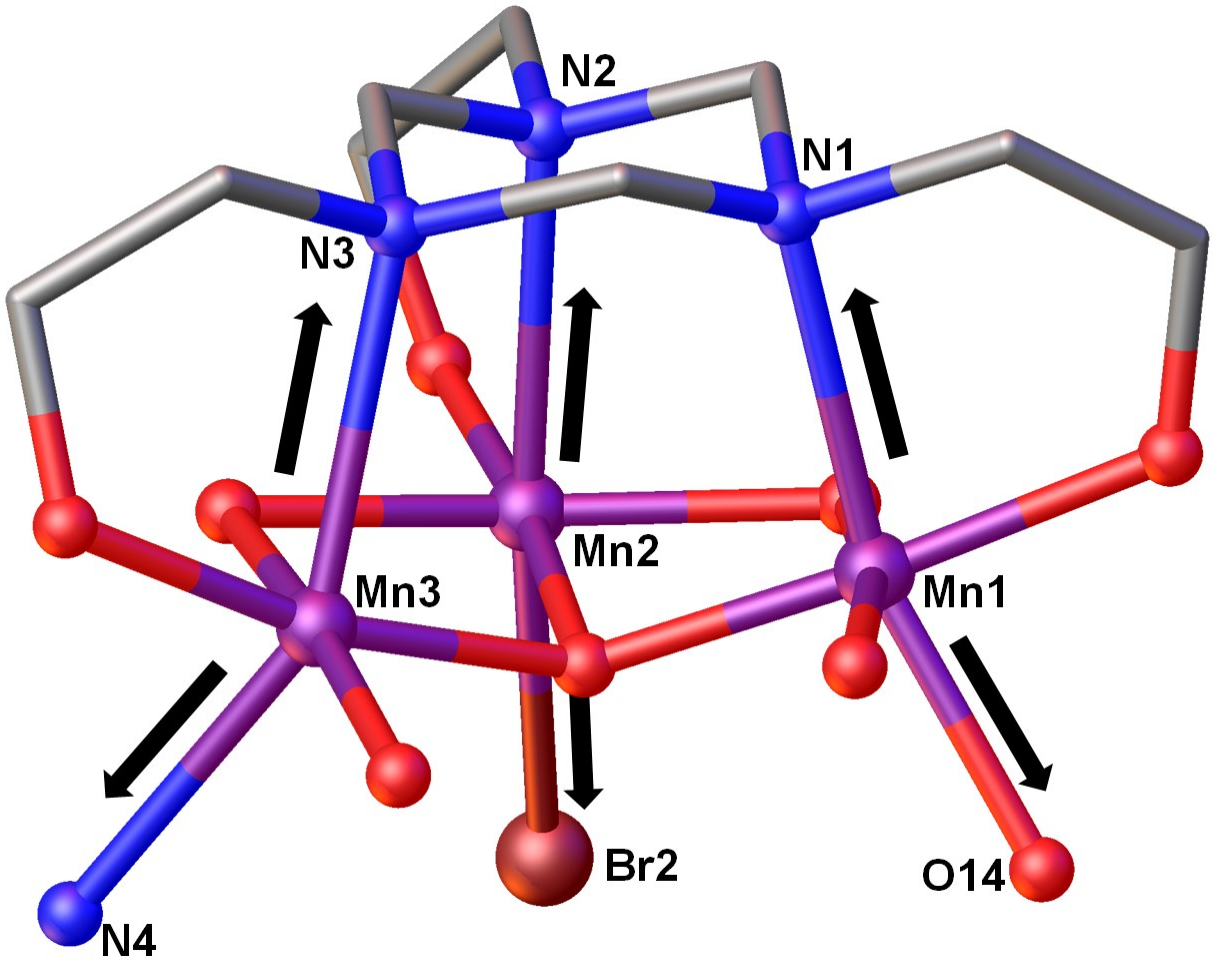

Figure S3. View of the L^{3-} ligand sitting above a $[Mn^{III}_3]$ triangle. The arrows highlight the Jahn-Teller axes. JT Bond lengths: Mn1-N1, 2.342(17) Å; Mn1-O14, 2.088(14) Å; Mn2-N2, 2.479(18) Å; Mn2-Br2, 2.084 Å; Mn3-N3, 2.511(18) Å; Mn3-N4, 2.463(19) Å . Colour code: Mn^{III} = purple, C = grey, O = red, N = dark blue, Br = brown. H atoms omitted for clarity.

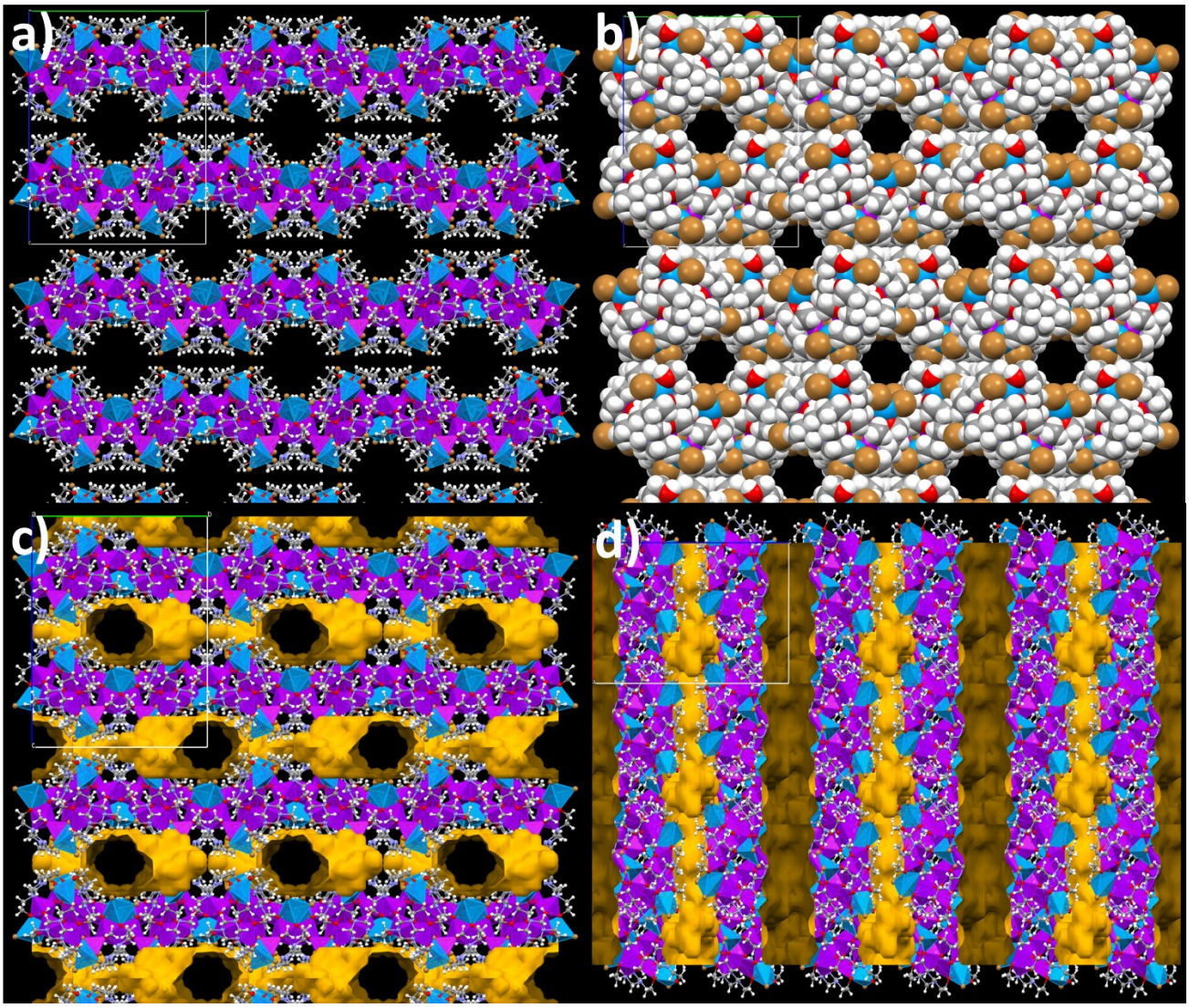

Figure S4. View of the extended structure of **1** in the *bc* plane in a) polyhedral and b) space-fill format. c) and d) show the solvent filled voids in yellow, viewed down the c) *a*-axis and d) *b*-axis.

Supplementary Information

Table S1. Pertinent bond lengths (Å) and angles (°) for **1**.

Mn1	**Mn2**	**Mn3**	**Mn4**	**Mn5**
Mn1 O1 1.951(16)	Mn2 O2 1.922(17)	Mn3 O3 1.925(15)	Mn4 O3 2.121(17)	Mn5 O6 1.966(13)
Mn1 O10 2.070(18)	Mn2 O4 2.010(16)	Mn3 O4 1.977(17)	Mn4 O5 2.115(19)	Mn5 O9 1.951(17)
Mn1 O11 1.904(13)	Mn2 O11 1.927(15)	Mn3 O11 1.909(15)	Mn4 O9 2.081(16)	Mn5 O12 1.887(14)
Mn1 O14 2.088(14)	Mn2 O15 1.971(15)	Mn3 O12 1.915(16)	Mn4 O12 2.195(15)	Mn5 O13 1.924(15)
Mn1 O15 2.036(19)	Mn2 N2 2.479(18)	Mn3 N3 2.511(18)	Mn4 Br1 2.608(5)	Mn5 N6 2.488(19)
Mn1 N1 2.342(17)	Mn2 Br2 2.804	Mn3 N4 2.463(19)		Mn5 N9 2.56(2)
Mn6	**Mn7**	**Mn8**	**Mn9**	
Mn6 O6 2.057(17)	Mn7 O8 1.938(15)	Mn8 O2 2.106(18)	Mn9 Br5 2.558(5)	
Mn6 O7 1.946(18)	Mn7 O10 1.945(13)	Mn8 O7 2.10(2)	Mn9 Br6 2.581(5)	
Mn6 O13 1.968(14)	Mn7 O13 1.851(14)	Mn8 Br2 2.825(5)	Mn9 O1 2.111(13)	
Mn6 O16 1.989(19)	Mn7 O14 2.129(18)	Mn8 Br3 2.553(5)	Mn9 O8 2.083(19)	
Mn6 N7 2.45(2)	Mn7 O16 1.948(14)	Mn8 Br4 2.546(6)	Mn9 O14 2.265(16)	
Mn6 Br2 2.784(5)	Mn7 N8 2.39(2)			

Mn1	**Mn2**	**Mn3**	**Mn4**	**Mn5**
Mn1 O1 Mn9 105.7(7)	Mn2 O2 Mn8 125.449	Mn3 O3 Mn4 99.8(6)	Mn4 O3 Mn3 99.8(6)	Mn5 O12 Mn4 96.9(7)
Mn1 O14 Mn7 94.8(7)	Mn2 O4 Mn3 97.2(6)	Mn3 O12 Mn4 97.6(6)	Mn4 O12 Mn3 97.6(6)	Mn5 O9 Mn4 98.7(8)
Mn1 O14 Mn9 96.1(6)	Mn2 O11 Mn1 101.0(7)	Mn3 O4 Mn2 97.2(6)	Mn4 O12 Mn5 96.9(7)	Mn5 O6 Mn6 96.5(7)
Mn1 O10 Mn7 101.2(7)	Mn2 O11 Mn3 102.4(6)	Mn3 O11 Mn2 102.4(6)	Mn4 O9 Mn5 98.7(8)	Mn5 O13 Mn6 100.9(7)
Mn1 O15 Mn2 95.1(8)	Mn2 Br2 Mn8 79.016	Mn3 O11 Mn1 131.6(8)		Mn5 O12 Mn3 153.7(8)
Mn1 O11 Mn3 131.6(8)	Mn2 Br2 Mn6 157.013	Mn3 O12 Mn5 153.7(8)		Mn5 O13 Mn7 132.461
Mn1 O11 Mn2 101.0(7)				
Mn6	**Mn7**	**Mn8**	**Mn9**	
Mn6 O6 Mn5 96.5(7)	Mn7 O8 Mn9 107.9(8)	Mn8 O2 Mn2 125.449	Mn9 O1 Mn1 105.7(7)	
Mn6 O13 Mn5 100.9(7)	Mn7 O14 Mn9 95.4(6)	Mn8 Br2 Mn2 79.016	Mn9 O14 Mn1 96.1(6)	
Mn6 O13 Mn7 100.7(6)	Mn7 O13 Mn6 100.7(6)	Mn8 O7 Mn6 122.4(11)	Mn9 O8 Mn7 107.9(8)	
Mn6 Br2 Mn8 78.37(14)	Mn7 O16 Mn6 96.7(7)	Mn8 Br2 Mn6 78.37(14)	Mn9 O14 Mn7 95.4(6)	
Mn6 O7 Mn8 122.4(11)	Mn7 O10 Mn1 101.2(7)			
Mn6 O16 Mn7 96.7(7)	Mn7 O14 Mn1 94.8(7)			

Supplementary Information

Table S2. Bond Valence Sum (BVS) parameters for the Mn ions in **1**.

metal VBS	d(M-L1)	d(M-L2)	d(M-L3)	d(M-L4)	d(M-L5)	d(M-L6)		r(0)	beta
Mn1	2.342	2.088	1.951	2.07	2.036	1.904	O	1.76	0.37
	-0.505	-0.328	-0.191	-0.31	-0.276	-0.144			

metal VBS	d(M-L1)	d(M-L2)	d(M-L3)	d(M-L4)	d(M-L5)	d(M-L6)		r(0)	beta
Mn5	-1.36486	-0.88649	-0.51622	0.837838	-0.74595	-0.38919	N	1.837	
	2.56	2.488	1.887	1.951	1.924	1.966	O	1.76	0.37
	0.255415	0.412101	0.596774	0.432645	0.474285	0.677606			
	-0.651	-0.127	-0.191	-0.164	-0.206				
M(Ox.State)	2.848827	-1.75946	-0.34324	-0.516216	-0.44324	-0.55676	N	1.837	

metal VBS	d(M-L1)	d(M-L2)	d(M-L3)	d(M-L4)	d(M-L5)	d(M-L6)		r(0)	beta
M(Ox.State)									
Mn2	2.479	1.971	1.927	1.922	2.01	2.804	O	1.76	0.37
	-0.642	-0.211	-0.167	-0.162	-0.25	-0.464	Br	2.34	
	-1.73514	-0.57027	-0.45135	-0.437838	-0.67568	-1.25405	N	1.837	
	0.176376	0.565373	0.636767	0.6454304	0.508813	0.285346			
M(Ox.State)	2.818105								

metal VBS	d(M-L1)	d(M-L2)	d(M-L3)	d(M-L4)	d(M-L5)	d(M-L6)		r(0)	beta
Mn3	2.511	2.463	1.977	1.909	1.915	2.121	O	1.76	0.37
	-0.674	-0.626	-0.217	-0.149	-0.155	-0.361			
	-1.82162	-1.69189	-0.58649	-0.402703	-0.41892	-0.97568	N	1.837	
	0.161763	0.184171	0.556278	0.6685108	0.657758	0.376938			
M(Ox.State)	2.605418								

metal VBS	d(M-L1)	d(M-L2)	d(M-L3)	d(M-L4)	d(M-L5)	d(M-L6)		r(0)	beta
Mn4	2.195	2.081	2.115	2.121	2.608		O	1.79	0.37
	-0.405	-0.291	-0.325	-0.331	-0.268		Br	2.34	
	-1.09459	-0.78649	-0.87838	-0.894595	-0.72432		N	1.837	
	0.334675	0.455442	0.415456	0.4087733	0.484652				
M(Ox.State)	2.098999								

metal VBS	d(M-L1)	d(M-L2)	d(M-L3)	d(M-L4)	d(M-L5)	d(M-L6)		r(0)	beta
Mn6	2.45	1.989	1.968	1.946	2.057	2.784	O	1.76	0.37
	-0.613	-0.229	-0.208	-0.186	-0.297	-0.444	Br	2.34	
	-1.65676	-0.61892	-0.56216	-0.502703	-0.8027	-1.2	N	1.837	
	0.190757	0.538526	0.569975	0.6048936	0.448116	0.3011947			
M(Ox.State)	2.527694								

metal VBS	d(M-L1)	d(M-L2)	d(M-L3)	d(M-L4)	d(M-L5)	d(M-L6)		r(0)	beta
Mn7	2.39	2.129	1.938	1.945	1.851	1.958	O	1.76	0.37
	-0.553	-0.369	-0.178	-0.185	-0.091	-0.198			

Supplementary Information

						0.53514			
	0.22434	0.368875	0.618115	0.6065307	0.781964	0.58559			
M(Ox.State)	3.185415								

metal VBS	d(M-L1)	d(M-L2)	d(M-L3)	d(M-L4)	d(M-L5)	d(M-L6)		r(0)	beta
Mn9	2.111	2.083	2.256	2.558	2.581	0	O	1.79	0.37
metal VBS	d(M-L1)	d(M-L2)	d(M-L3)	d(M-L4)	d(M-L5)	d(M-L6)		r(0)	beta
Mn8	-0.86757	-0.79187	-1.25946	-0.58958	-0.65825	0	O	1.79	0.37
	0.419972	0.452987	0.283207	0.5547709	0.521345	1	Br	2.34	
M(Ox.State)	2.232884	-0.85676	-0.57568	-0.556757	-1.31081	0			
	0.419972	0.424537	0.562325	0.5730646	0.269601	1			
M(Ox.State)	2.249499								

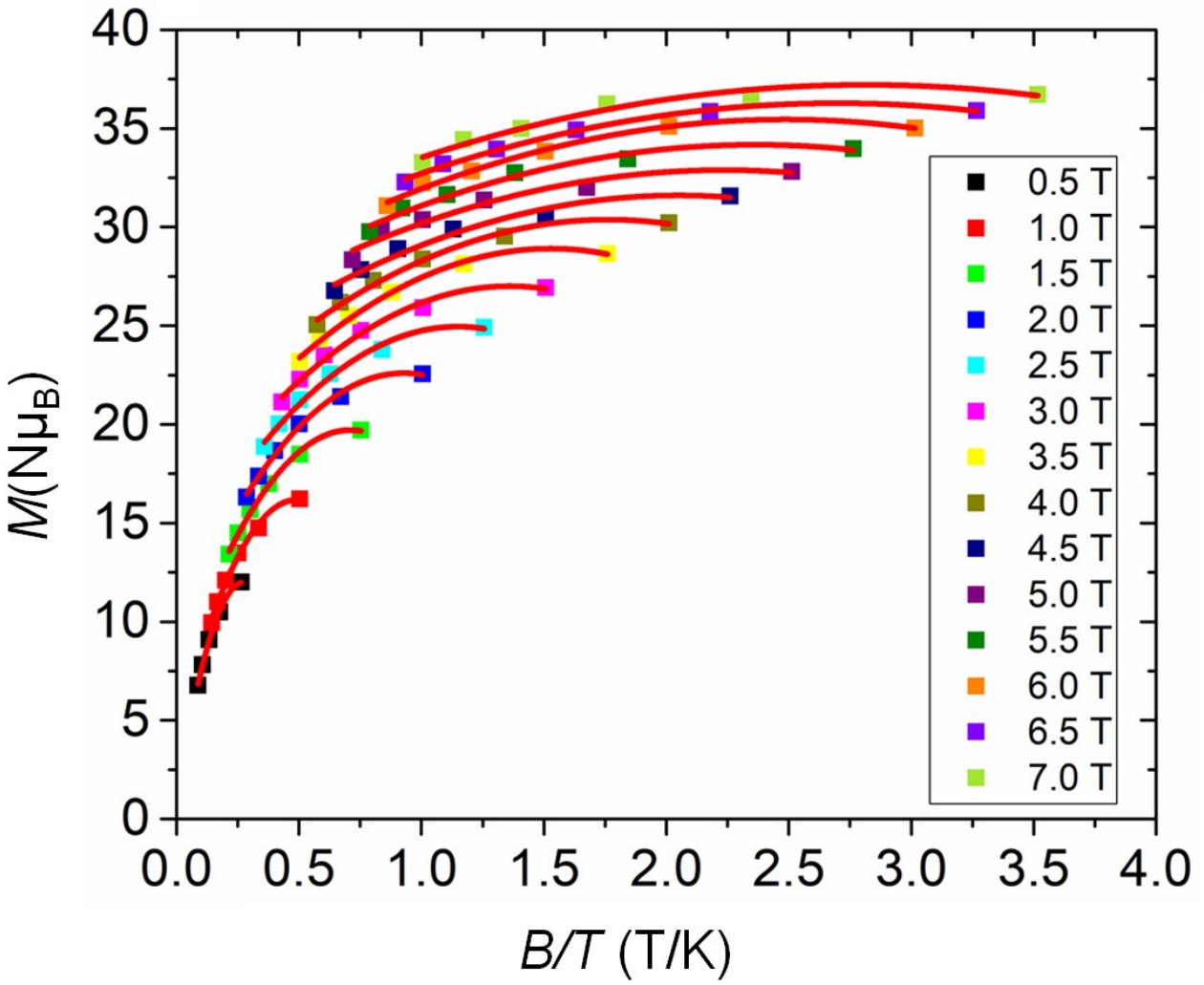

Figure S5. Plot of the reduced magnetisation (*M*) vs (*B*/*T*) for compound **1** in *B* = 0.5-7 T. The red lines are a guide to the eye, not a fit of the data.

COMPUTATIONAL DETAILS

We have used density functional theory (DFT) in the Gaussian 16 suite to estimate the magnetic exchange coupling constants (J_1-J_6) for **1**.[2] We have performed calculations on model complex **1a** based on the ASU of **1** (Mn_9, Figure S7). For the calculation of each interaction we have used the diamagnetic substitution method by keeping only the two paramagnetic ions of interest and replacing all others with diamagnetic ions (Ga^{III} and Zn^{II} for Mn^{III} and Mn^{II}, respectively). By doing so, we keep the ligand field around the paramagnetic metals ions identical to **1**. This method is known to yield reliable magnetic exchange coupling values for molecular systems with relatively small magnetic interactions.[3] Noodleman's broken symmetry approach[4] has been used to estimate the magnetic exchange coupling constants. We have used the B3LYP functional[5] together with Ahlrichs TZV basis set[6] for Mn, Ga, Zn; the SDD basis set[7] (which combines DZ with the Stuttgart-Dresden ECP basis set) for Br and the 6-31G** basis set[8] for O, N, C and H. This methodology has been known to yield excellent estimates of *J* values for 3d metal clusters.[3b,9]

Table S3. DFT computed magnetic exchange interactions together with pertinent structural parameters for **1**.

Exchange		Bridging groups	Mn···Mn Dist. [Å]	Avg. Mn-O Dist. [Å]	Avg. Mn-O-Mn angle [^{o}]	*J* cm^{-1}
J_1	Mn_{12}	μ_3-O, μ-OR	2.94	1.94	99	-10
	Mn_{23}	μ_3-O, μ-OR	3.00	1.98	99	
	Mn_{56}	μ_3-O, μ-OR	2. 99	1.96	100	
	Mn_{67}	μ_3-O, μ-OR	2.96	1.97	98	
J_2	Mn_{13}	μ_3-O	3.46	1.89	133	-9
	Mn_{35}	μ_3-O	3.52	1.90	136	
	Mn_{57}	μ_3-O	3.48	1.90	132	
J_3	Mn_{17}	μ-OH, μ_3-OR	3.10	2.03	98	+8
J_4	Mn_{34}	μ_3-O, μ-OR	3.06	2.03	98	+1
	Mn_{45}	μ_3-O, μ-OR	3.10	2.04	99	
J_5	Mn_{19}	μ-OR, μ_3-OR	3.25	2.11	102	+2
	Mn_{79}	μ-OR, μ_3-OR	3.24	2.10	101	
J_6	Mn_{68}	μ-Br, μ-OR	3.58	2.42	102	+2

Table S4. DFT computed overlap integral (OI) values for J_1-J_6. Here α and β signify spin-up and spin-down orbitals, respectively. $\sum|S_{a(3d)b(3d)}|$ represents the total OIs and $\sum|S_{a(3d)b(3d)}|/n$ represents the average total OIs between Mn^{III}-Mn^{III}/Mn^{II}-Mn^{III} SOMOs. n = number of possible OIs between the SOMOs (for $3d^4$-$3d^4$ systems, n = 16 and for $3d^5$-$3d^4$ systems, n = 20). Red and yellow highlighted numbers represent strong and intermediate interactions, respectively.

						$\sum\|S_{a(3d)b(3d)}\|$	$\sum\|S_{a(3d)b(3d)}\|/n$
J_1	β(→)/α(↓)	d_{xz}	d_{xy}	d_{yz}	d_z^2		
	d_{xy}	0.025	0.023	0.026	0.069	0.708	0.044
	d_{xz}	0.066	0.027	0.001	0.001		
	d_{yz}	0.049	0.014	0.057	0.001		
	d_z^2	0.137	0.072	0.100	0.040		
J_2	β(→)/α(↓)	d_{xz}	d_{yz}	d_{xy}	d_z^2		
	d_{xy}	0.054	0.012	0.044	0.042	0.572	0.036
	d_{xz}	0.005	0.057	0.001	0.058		
	d_{yz}	0.005	0.006	0.022	0.135		
	d_z^2	0.018	0.032	0.003	0.078		
J_3	β(→)/α(↓)	d_{xz}	d_{yz}	d_{xy}	d_z^2		
	d_{xy}	0.003	0.004	0.052	0.070	0.338	0.021
	d_{xz}	0.002	0.005	0.015	0.016		
	d_{yz}	0.016	0.012	0.019	0.012		
	d_z^2	0.068	0.009	0.024	0.011		
J_4	β(→)/α(↓)	d_{xy}	d_{xz}	d_{yz}	d_z^2		
	d_{xz}	0.027	0.081	0.052	0.036	0.624	0.031
	d_{yz}	0.030	0.030	0.020	0.018		
	d_{xy}	0.036	0.008	0.023	0.079		
	d_z^2	0.013	0.048	0.058	0.045		
	$d_{x^2-y^2}$	0.004	0.006	0.009	0.001		
J_5	β(→)/α(↓)	d_{xy}	d_{xz}	d_{yz}	d_z^2		
	d_{xz}	0.012	0.017	0.011	0.068	0.467	0.023
	d_{xy}	0.011	0.088	0.011	0.010		
	d_{yz}	0.038	0.032	0.026	0.004		
	d_z^2	0.006	0.000	0.031	0.025		
	$d_{x^2-y^2}$	0.045	0.038	0.020	0.057		
J_6	β(→)/α(↓)	d_{xz}	d_{xy}	d_{yz}	d_z^2		
	d_{xy}	0.025	0.001	0.007	0.004	0.490	0.025
	d_{xz}	0.001	0.027	0.009	0.009		
	$d_{x^2-y^2}$	0.009	0.039	0.017	0.013		
	d_{yz}	0.082	0.035	0.012	0.016		
	d_z^2	0.015	0.026	0.038	0.105		

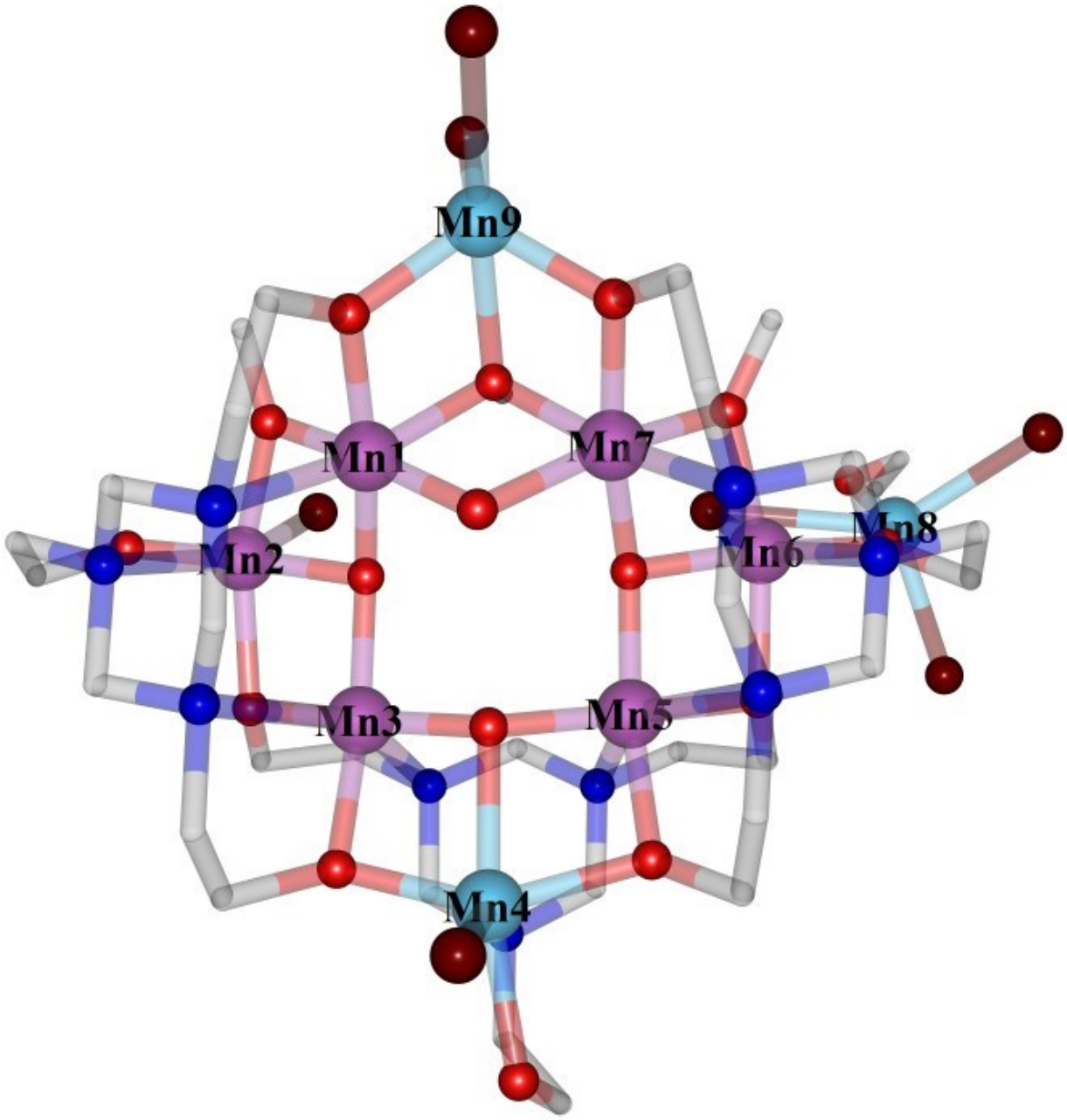

Figure S6. The structure of model complex **1a** on which DFT calculations were performed to estimate the magnetic exchange coupling constants. H-atoms are removed for clarity (except the μ-OH bridging group). Colour code is the same as for Figure 2.

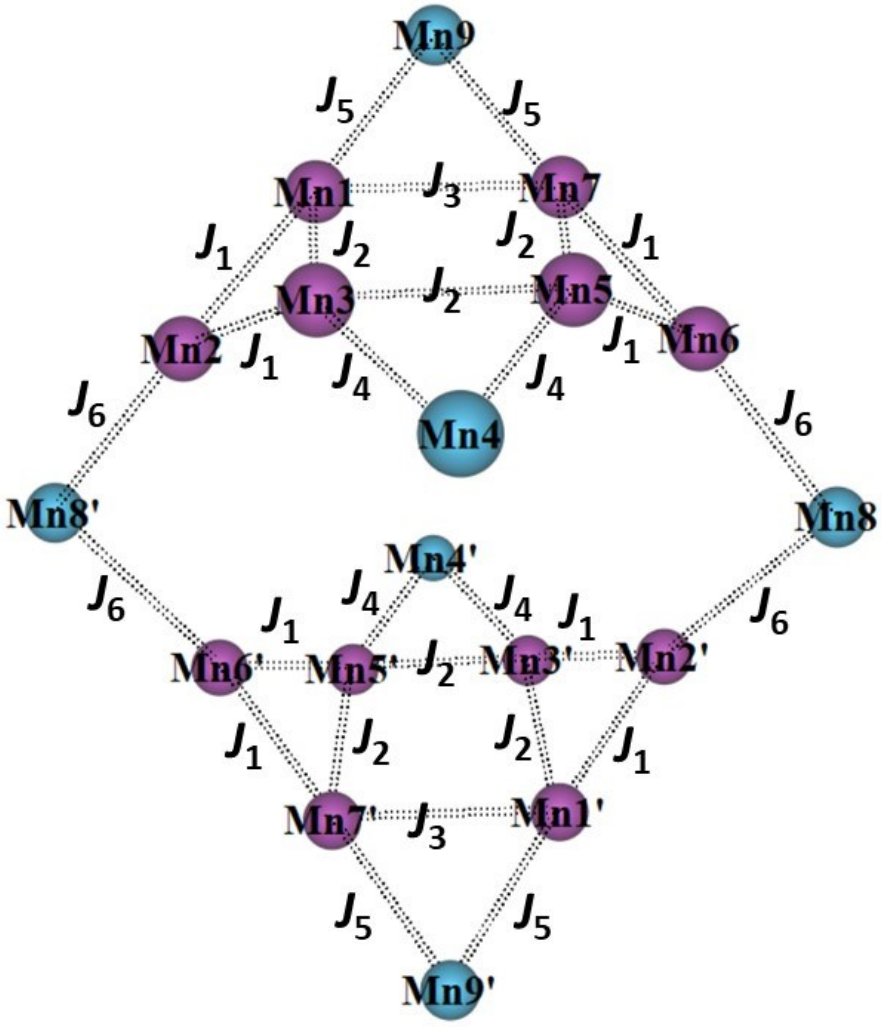

$$\hat{H} = -2J_1(\hat{S}_{Mn1}\hat{S}_{Mn2} + \hat{S}_{Mn2}\hat{S}_{Mn3} + \hat{S}_{Mn5}\hat{S}_{Mn6} + \hat{S}_{Mn6}\hat{S}_{Mn7} + \hat{S}_{Mn1'}\hat{S}_{Mn2'} + \hat{S}_{Mn2'}\hat{S}_{Mn3'} + \hat{S}_{Mn5'}\hat{S}_{Mn6'} + \hat{S}_{Mn6'}\hat{S}_{Mn7'})$$
$$-2J_2(\hat{S}_{Mn1}\hat{S}_{Mn3} + \hat{S}_{Mn3}\hat{S}_{Mn5} + \hat{S}_{Mn5}\hat{S}_{Mn7} + \hat{S}_{Mn1'}\hat{S}_{Mn3'} + \hat{S}_{Mn3'}\hat{S}_{Mn5'} + \hat{S}_{Mn5'}\hat{S}_{Mn7'}) -2J_3(\hat{S}_{Mn1}\hat{S}_{Mn7} + \hat{S}_{Mn1'}\hat{S}_{Mn7'})$$
$$-2J_4(\hat{S}_{Mn3}\hat{S}_{Mn4} + \hat{S}_{Mn4}\hat{S}_{Mn5} + \hat{S}_{Mn3'}\hat{S}_{Mn4'} + \hat{S}_{Mn4'}\hat{S}_{Mn5'}) -2J_5(\hat{S}_{Mn1}\hat{S}_{Mn9} + \hat{S}_{Mn7}\hat{S}_{Mn9} + \hat{S}_{Mn1'}\hat{S}_{Mn9'} + \hat{S}_{Mn7'}\hat{S}_{Mn9'})$$
$$-2J_6(\hat{S}_{Mn2}\hat{S}_{Mn8} + \hat{S}_{Mn6}\hat{S}_{Mn8} + \hat{S}_{Mn2'}\hat{S}_{Mn8'} + \hat{S}_{Mn6'}\hat{S}_{Mn8'})$$

Figure S7. Schematic representation of the six different exchange interactions present in **1**, together with the exchange part of the corresponding spin-Hamiltonian.

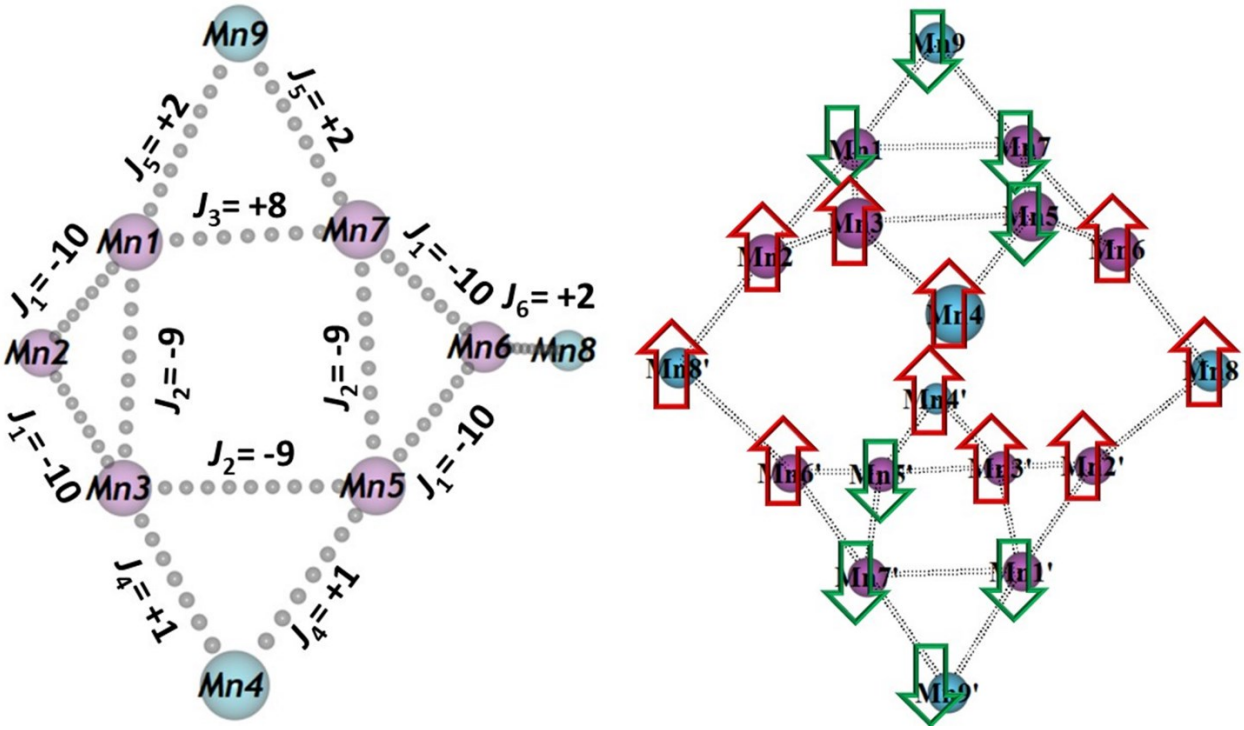

Figure S8. (left) DFT calculated magnetic exchange interactions (J_1-J_6 / cm^{-1}) for the model **1a** (the asymmetric unit). (right) Schematic representation of spin orientation for **1** based on the DFT calculated *J* values. Red and green arrows represent "spin-up" and "spin-down", respectively.

(a)

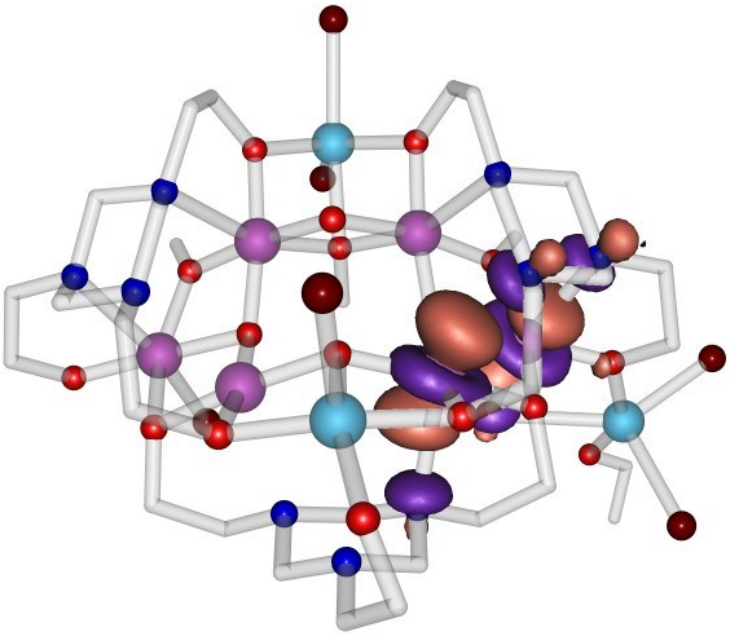

(b)

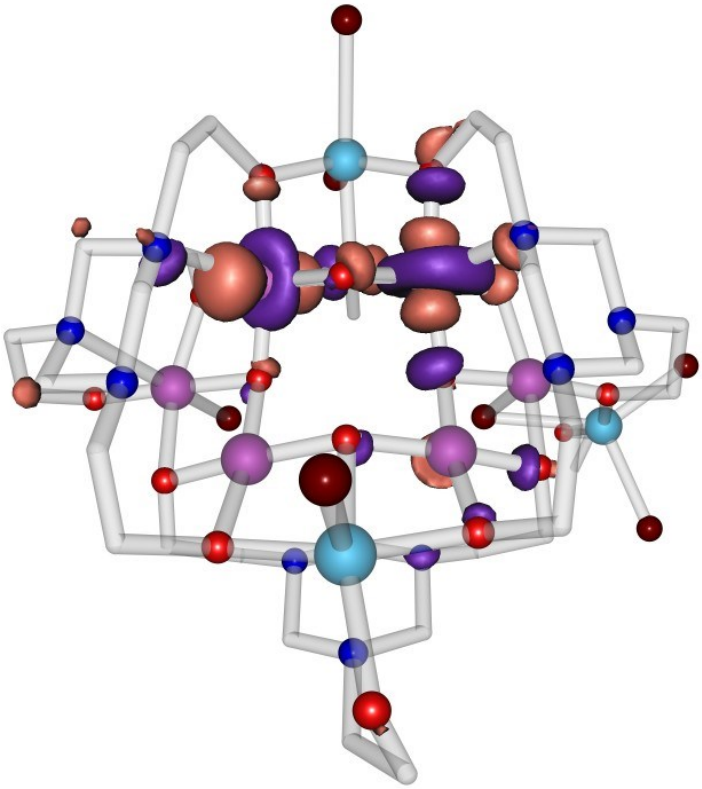

Figure S9. Schematic presentation of Jahn-Teller axis for (a) {Mn5-Mn6, J_1} and (b) {Mn1-Mn7, J_3} centres within the ASU. For J_1 the Jahn-Teller axis of both Mn^{III} ions are found to be collinear and are perpendicular to the bridging

plane of the dimer (Type I). For J_3 interaction, the Jahn-Teller axes of Mn^{III} ions are perpendicular to each other with one lying parallel to the bridging plane and the other perpendicular to the bridging plane (Type III).[10]

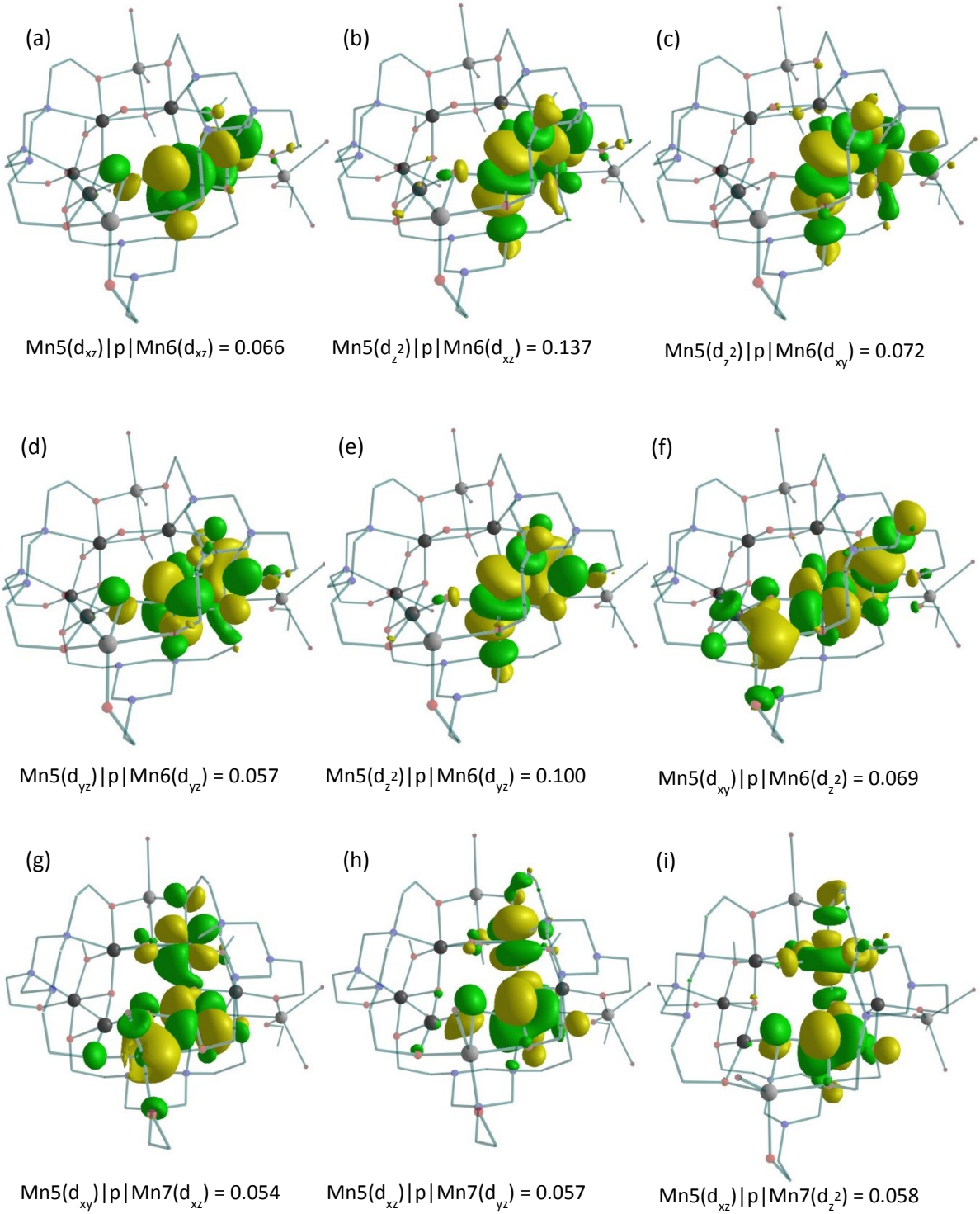

Supplementary Information

(j)

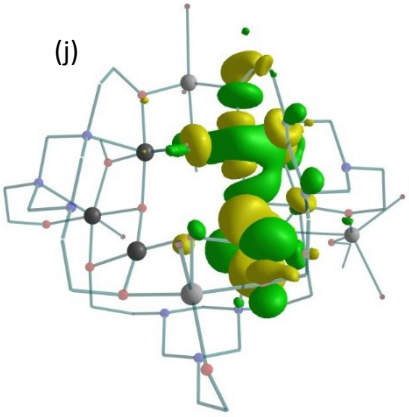

$Mn5(d_{yz})|p|Mn7(d_{z^2}) = 0.135$

(k)

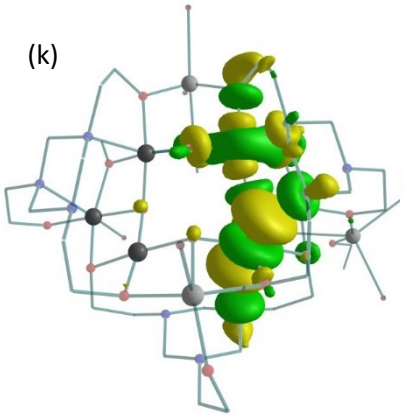

$Mn5(d_{z^2})|p|Mn7(d_{z^2}) = 0.078$

(l)

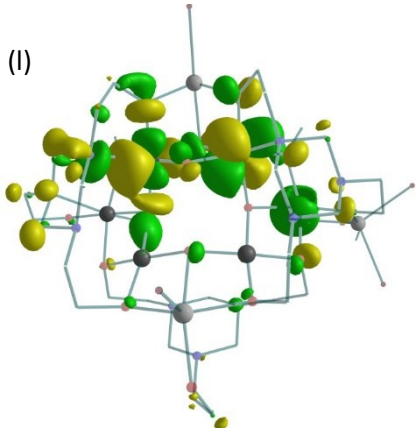

$Mn1(d_{z^2})|p|Mn7(d_{xz}) = 0.068$

(m)

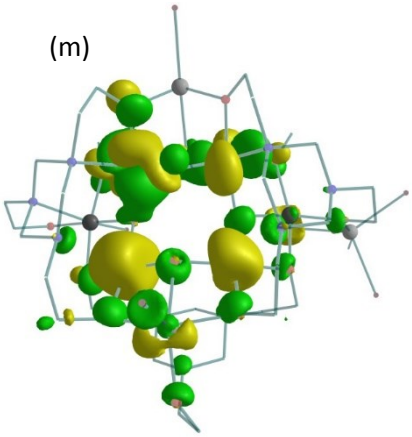

$Mn1(d_{xy})|p|Mn7(d_{xy}) = 0.052$

(n)

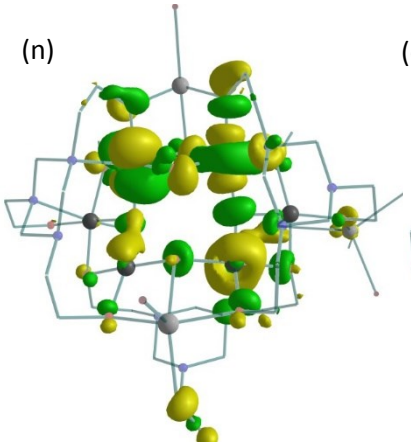

$Mn1(d_{xy})|p|Mn7(d_{z^2}) = 0.070$

(o)

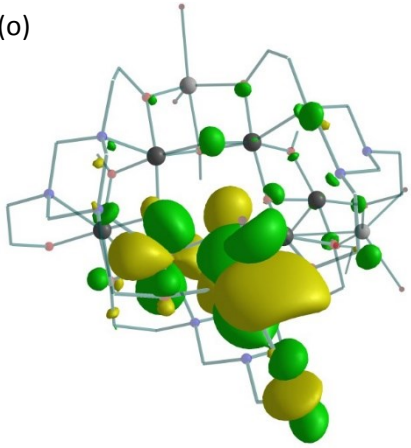

$Mn4(d_{xz})|p|Mn3(d_{xz}) = 0.081$

(p)

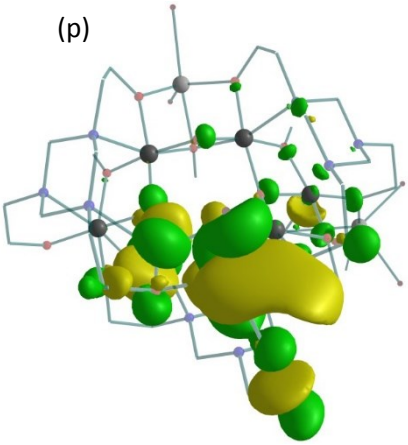

$Mn4(d_{xz})|p|Mn3(d_{yz}) = 0.052$

(q)

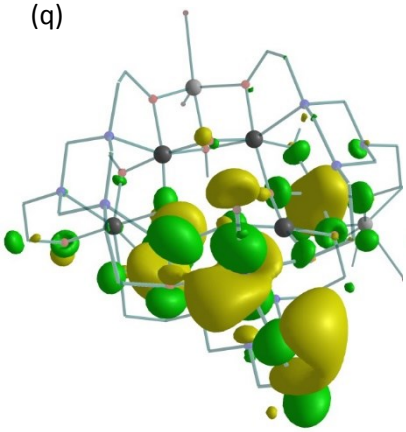

$Mn4(d_{z^2})|p|Mn3(d_{yz}) = 0.058$

(r)

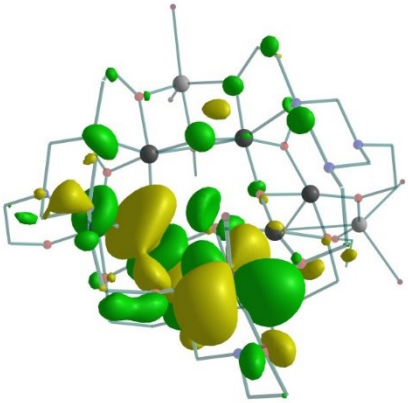

$Mn4(d_{xy})|p|Mn3(d_{z^2}) = 0.079$

Supplementary Information

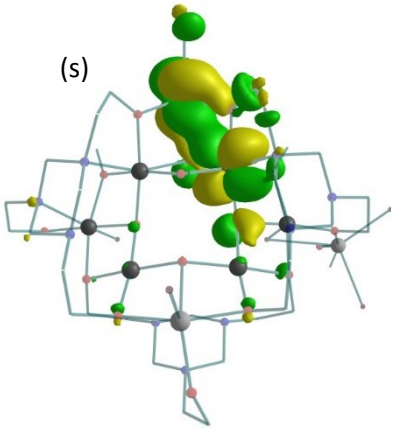

$Mn9(d_{xy})|p|Mn7(d_{xz}) = 0.088$

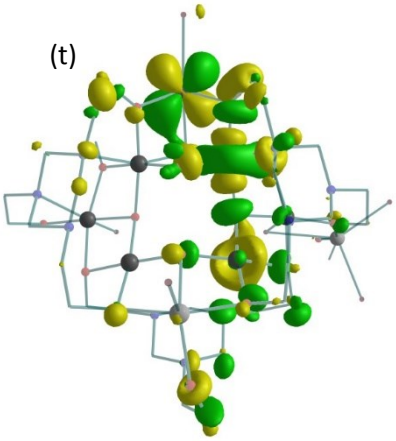

$Mn9(d_{xz})|p|Mn7(d_{z^2}) = 0.068$

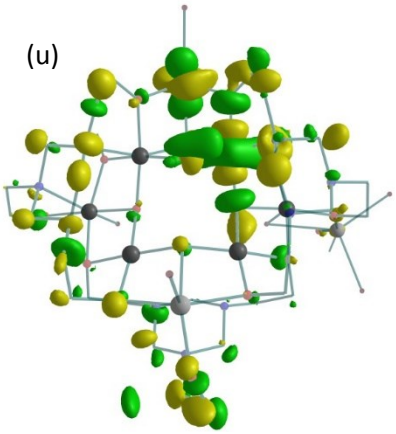

$Mn9(d_{x^2-y^2})|p|Mn7(d_{z^2}) = 0.057$

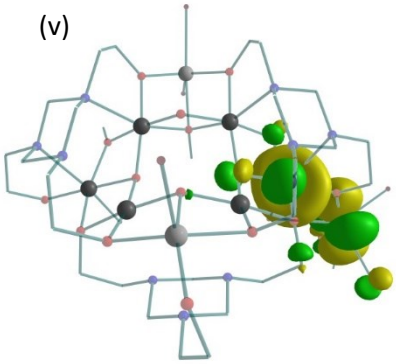

$Mn8(d_{yz})|p|Mn6(d_{xz}) = 0.082$

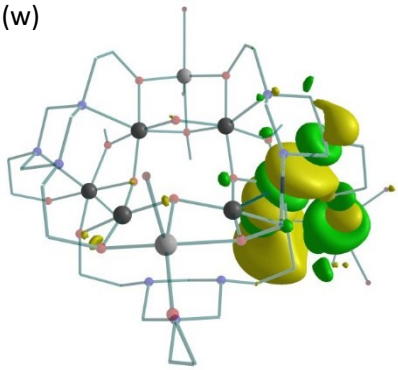

$Mn8(d_{z^2})|p|Mn6(d_{z^2}) = 0.105$

Figure S10. DFT calculated strong and intermediate overlap integrals corresponding to (a-f) J_1; (g-k) J_2; (l-n) J_3; (o-r) J_4; (s-u) J_5 and (v-w) J_6.

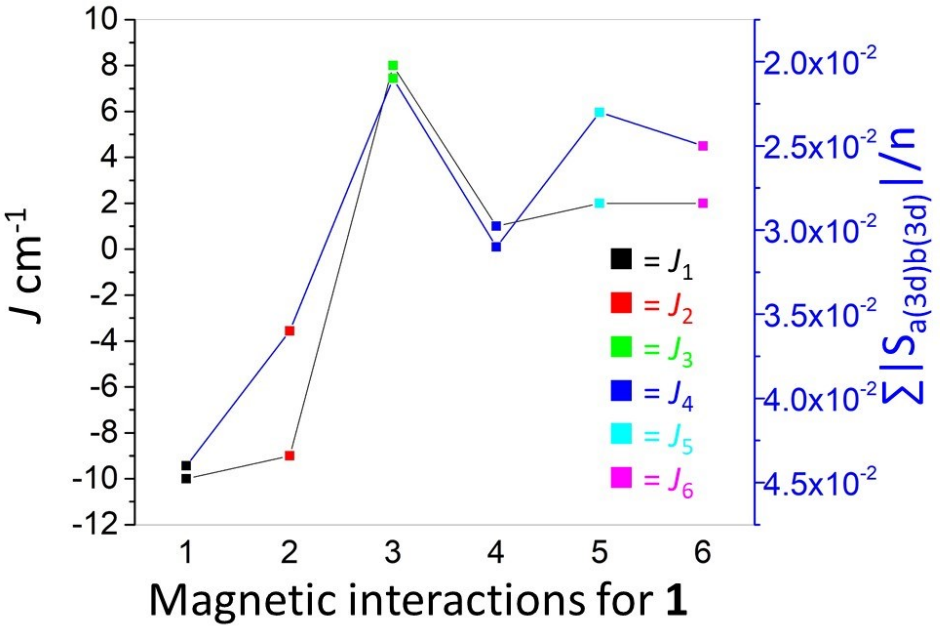

Figure S11. Plot of J versus average total overlap integral ($\sum|S_{a(3d)b(3d)}|/n$) with respect to the calculated magnetic exchange interactions for **1**. The magnitude and the sign of the magnetic exchange interaction can be correlated to the calculated average total overlap integral. The smaller the average total overlap integral, the larger the ferromagnetic interaction and vice versa.[3a]

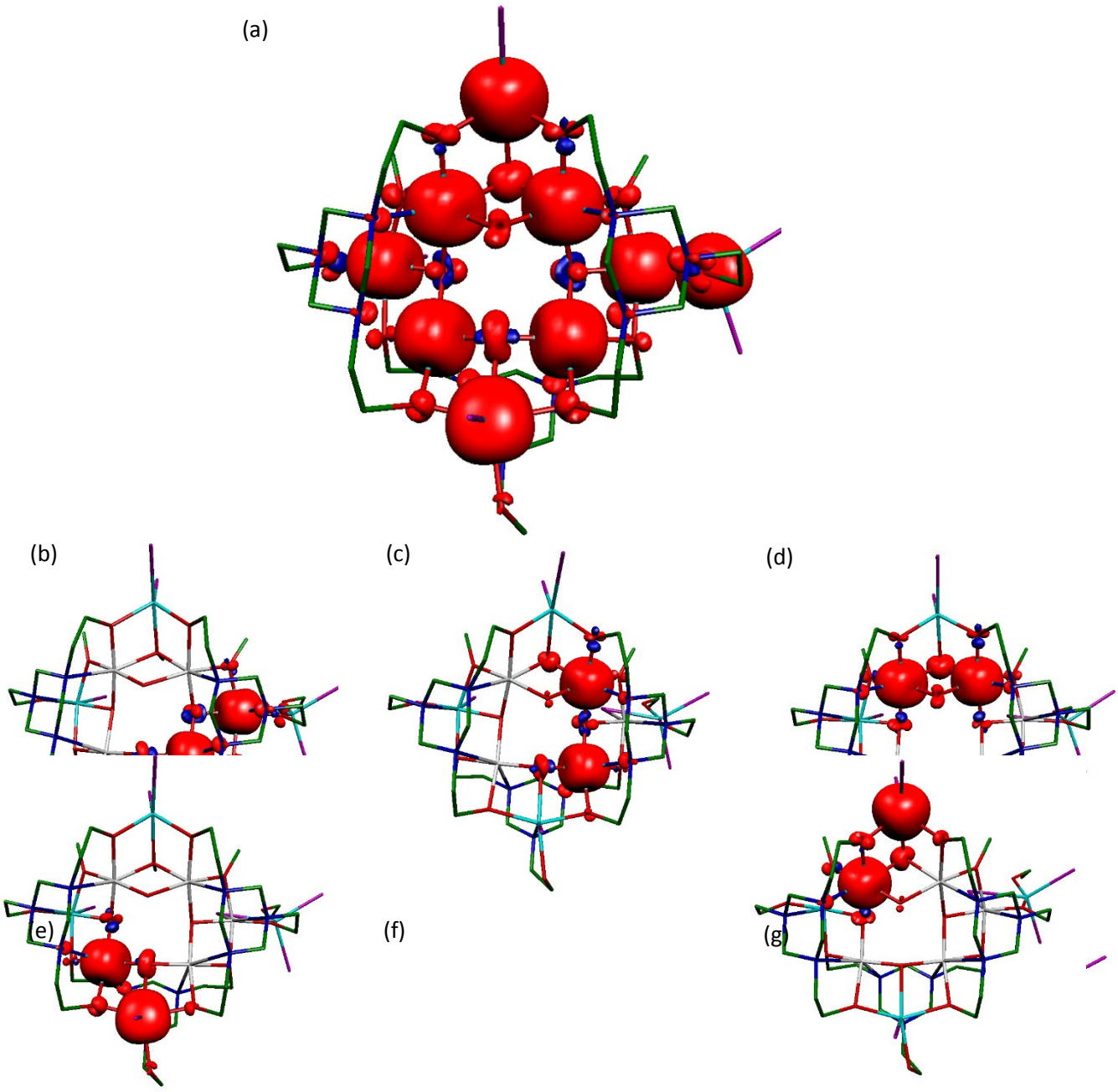
(a)
(b)
(c)
(d)
(e)
(f)
(g)

Figure S12. DFT calculated spin density plots for (a) model **1a** and (b-g) diamagnetic substituted models for J_1-J_6, respectively. The isodensity surfaces shown reflect a value of 0.01 e -/bohr^3. The red and blue surfaces denote positive and negative spin density, respectively.

References:

1. N. T. Johnson, P. G. Waddell, W. Clegg and M. R. Probert, *Crystals*, 2017, **7**, 360.
2. M. J. Frisch, G. W. Trucks, H. B. Schlegel, G. E. Scuseria, M. A. Robb, J. R. Cheeseman, G. Scalmani, V. Barone, G. A. Petersson, H. Nakatsuji, X. Li, M. Caricato, A. V. Marenich, J. Bloino, B. G. Janesko, R. Gomperts, B. Mennucci, H. P. Hratchian, J. V. Ortiz, A. F. Izmaylov, J. L. Sonnenberg, Williams, F. Ding, F. Lipparini, F. Egidi, J. Goings, B. Peng, A. Petrone, T. Henderson, D. Ranasinghe, V. G. Zakrzewski, J. Gao, N. Rega, G. Zheng, W. Liang, M. Hada, M. Ehara, K. Toyota, R. Fukuda, J. Hasegawa, M. Ishida, T. Nakajima, Y. Honda, O. Kitao, H. Nakai, T. Vreven, K. Throssell, J. A. Montgomery Jr., J. E. Peralta, F. Ogliaro, M. J. Bearpark, J. J. Heyd, E. N. Brothers, K. N. Kudin, V. N. Staroverov, T. A. Keith, R. Kobayashi, J. Normand, K. Raghavachari, A. P. Rendell, J. C. Burant, S. S. Iyengar, J. Tomasi, M. Cossi, J. M. Millam, M. Klene, C. Adamo, R. Cammi, J. W. Ochterski, R. L. Martin, K. Morokuma, O. Farkas, J. B. Foresman and D. J. Fox, Gaussian, Inc., Wallingford CT, 2016.
3. a) M. Coletta, S. Sanz, D. J. Cutler, S. J. Teat, K. J. Gagnon, M. K. Singh, E. K. Brechin and S. J. Dalgarno, *Dalton Trans.*, 2020, **49**, 14790-14797; b) A. E. Dearle, D. J. Cutler, H. W. L. Fraser, S. Sanz, E. Lee, S. Dey, I. F. Diaz-Ortega, G. S. Nichol, H. Nojiri, M. Evangelisti, G. Rajaraman, J. Schnack, L. Cronin and E. K. Brechin, *Angew. Chem. Int. Ed.*, 2019, **58**, 16903-16906.
4. L. Noodleman, *J. Chem. Phys.*, 1981, **74**, 5737.
5. a) A. D. Becke, *Phys. Rev. A*, 1988, **38**, 3098-3101; b) A. D. Becke, *J. Chem. Phys.*, 1993, **98**, 5648; c) C. Lee, W. Yang and R. G. Parr, *Phys. Rev. B: Condens. Matter Mater. Phys.*, 1988, **37**, 785.
6. a) A. Schafer, H. Horn and R. Ahlrichs, *J. Chem. Phys.*, 1992, **97**, 2571-2577; b) A. Schäfer, C. Huber and R. Ahlrichs, *J. Chem. Phys.*, 1994, **100**, 5829; c) G. E. Scuseria and H. F. Schäfer, *J. Chem. Phys.*, 1989, **90**, 3700.
7. A. Bergner, M. Dolg, W. Küchle, H. Stoll and H. Preuß, *Mol. Phys.*, 1993, **80**, 1431-1441.
8. V. A. Rassolov, J. A. Pople, M. A. Ratner and T. L. Windus, *J. Chem. Phys.*, 1998, **109**, 1223-1229.
9. a) M. K. Singh, *Dalton Trans.*, 2020, **49**, 4539-4548; b) M. K. Singh and G. Rajaraman, *Inorg. Chem.*, 2019, **58**, 3175-3188; c) M. K. Singh and G. Rajaraman, *Chem. Eur. J.*, 2015, **21**, 980-983; d) J. Caballero-Jiménez, F. Habib, D. Ramírez-Rosales, R. Grande-Aztatzi, G. Merino, I. Korobkov, M. K. Singh, G. Rajaraman, Y. Reyes-Ortega and M. Murugesu, *Dalton Trans*, 2015, **44**, 8649; e) C. McDonald, S. Sanz, E. K. Brechin, M. K. Singh, G. Rajaraman, D. Gaynor and L. F. Jones, *RSC Adv.*, 2014, **4**, 38182.
10. N. Berg, T. Rajeshkumar, S. M. Taylor, E. K. Brechin, G. Rajaraman and L. F. Jones, *Chem. - Eur. J.*, 2012, **18**, 5906.